Pure Appl. Geophys. 173 (2016), 463–485

DOI 10.1007/s00024-015-1119-5

Pure and Applied Geophysics

Scenario-Based Validation of Moderate Resolution DEMs Freely Available for Complex Himalayan Terrain

Mritunjay Kumar Singh,[1,2] R. D. Gupta,[2] Snehmani,[1] Anshuman Bhardwaj,[1] and Ashwagosha Ganju[1]

Abstract—Accuracy of the Digital Elevation Model (DEM) affects the accuracy of various geoscience and environmental modelling results. This study evaluates accuracies of the Advanced Spaceborne Thermal Emission and Reflection Radiometer (ASTER) Global DEM Version-2 (GDEM V2), the Shuttle Radar Topography Mission (SRTM) X-band DEM and the NRSC Cartosat-1 DEM V1 (CartoDEM). A high resolution (1 m) photogrammetric DEM (ADS80 DEM), having a high absolute accuracy [1.60 m linear error at 90 % confidence (LE90)], resampled at 30 m cell size was used as reference. The overall root mean square error (RMSE) in vertical accuracy was 23, 73, and 166 m and the LE90 was 36, 75, and 256 m for ASTER GDEM V2, SRTM X-band DEM and CartoDEM, respectively. A detailed error analysis was performed for individual as well as combinations of different classes of aspect, slope, land-cover and elevation zones for the study area. For the ASTER GDEM V2, forest areas with North facing slopes (0°–5°) in the 4th elevation zone (3773–4369 m) showed minimum LE90 of 0.99 m, and barren with East facing slopes (>60°) falling under the 2nd elevation zone (2581–3177 m) showed maximum LE90 of 166 m. For the SRTM DEM, pixels with South-East facing slopes of 0°–5° in the 4th elevation zone covered with forest showed least LE90 of 0.33 m and maximum LE90 of 521 m was observed in the barren area with North-East facing slope (>60°) in the 4th elevation zone. In case of the CartoDEM, the snow pixels in the 2nd elevation zone with South-East facing slopes of 5°–15° showed least LE90 of 0.71 m and maximum LE90 of 1266 m was observed for the snow pixels in the 3rd elevation zone (3177–3773 m) within the South facing slope of 45°–60°. These results can be highly useful for the researchers using DEM products in various modelling exercises.

Key words: DEM, ASTER GDEM, SRTM X-band DEM, NRSC CartoDEM, Slope, Aspect, Land cover, Accuracy, Error, Remote sensing, GIS.

1. Introduction

Maune *et al.* (2001) defined Digital elevation model (DEM) as a generic term normally implied for the elevation of bare earth without vegetation and buildings. Freely available height models (i.e., SRTM DEM, ASTER GDEM, and NRSC CartoDEM) derived from satellite remote sensing data sets are actually Digital Surface Models (DSMs) and include the elevation of reflective earth surface, including buildings and vegetation. However, they are called DEM by the data distribution agencies. Hence, adopting the same pattern, we are using the term DEM for the used height models in this study which are actually DSMs by definition.

DEM is a key element in today's digital geoscience world to understand and to explore the landscape of the earth surface (Pandit *et al.* 2014). DEM and its derived products (slope, aspect, curvature, drainage pattern and others) provide basic terrain-related information. These products are used as inputs to various studies like, avalanche (Snehmani *et al.* 2013), glacier (Snehmani *et al.* 2014) and flood mapping (Bhatt and Ahmed 2014), terrain visualization (Zhang *et al.* 2004), geomorphometry (Yadav *et al.* 2014), meteorological studies (Thornton *et al.* 1997), mass movement (Pradhan and Youssef 2010), runoff (Huss *et al.* 2008) and hydrological modelling (Maathuis and Wang 2006). An accurate DEM is the basic requirement for physiographic rectification as well as co-registration of temporal remotely sensed images, acquired with diverse incidence or sun elevation angles (Kaab 2005). Owing to such reliance of these mapping and modelling exercises on DEM and its by-products, the performance of models varies widely based on the accuracy of the DEM used (Zhang and Montgomery 1994). Thus, it is essential to consider the accuracy of the topographic data used

[1] Snow and Avalanche Study Establishment, Defence Research and Development Organization (DRDO), Him Parisar, Sector-37A, Chandigarh 160 036, India. E-mail: jay_rsgis@yahoo.co.in

[2] Motilal Nehru National Institute of Technology (MNNIT), Allahabad, UP 211 004, India.

in various geoscientific applications (Chen 2010). It is unfortunate that maximum users of DEMs are uninformed about the used DEM's accuracy and they ignore the influences of errors on the resultant derivatives, such as slope, aspect, curvature (Aguilar *et al*. 2010a). Hence, it is very important to acquire the information about spatial resolution, precision and accuracy of the used DEMs before any type of geoscientific modelling application (Holmes *et al*. 2000).

Usually, accuracy measures are based on the hypothesis that errors follow a normal dispersal (Saxena and Singh 2005; Toschi *et al*. 2015). However, it should be revised carefully. The historical idea was that errors were additive and nearly independent of the method of measurement. But, in most of the instances, this is not true with DEM as objects above the terrain, such as vegetation and buildings are ignored during the filtering process, especially in the case of complex mountainous terrain. Thus, the accuracy of DEMs depends on several factors such as the source and technique of measuring elevation data, the density and distribution of sampling points, methods of the DEM creation, and the precision in the representation of the elevation data along with the topographic complexity of the corresponding landscape (Chang and Tsai 1991; Gong *et al*. 2000). Considering all these factors, reference data in adequately large number are crucial for validating DEMs (Höhle and Höhle 2009).

There are several freely accessible DEMs such as the Global Topographic (GTOPO) DEM ($\sim$1 km global), the SRTM C-band DEM with spatial resolution of 30 m for USA and 90 m for other areas (Gorokhovich and Voustianiouk 2006), the SRTM X-band DEM (30 m global), the ASTER GDEM V2 (30 m global) and the CartoDEM (30 m for India only). Many attempts have been made for checking the vertical accuracy of various DEMs. For example, Krupnlk (2000) examined the accuracy and reliability of the automatically generated DEMs from the SPOT (Societé Pour l'Observation de la Terre) images for different kind of land covers, such as desert, agricultural, urban, and mountainous terrain with respect to the manually measured DEMs. They carefully marked out the areas that indicated failures of the automatic DEM generation procedure, further, predicting and improving the quality of the resulting DEMs. Miliaresis and Paraschou (2005) assessed vertical accuracy of SRTM DTED (Digital Terrain Elevation Data) level 1 product with respect to topographic maps at scale 1:250,000 for Crete Island (Southern Greece). They found the vertical accuracy of the SRTM product to be terrain class dependent. The greater mean error was observed for SW, W and NW aspect regions, while overall accuracy (RMSE) approached 25 m which was far more than the specified 16 m in the mission specification document. Kiel *et al.* (2006) analysed Shuttle Radar Topography Mission (SRTM) water surface elevation data in both X and C bands, to assess the capacity of interferometric radar for future surface water missions. Su and Bork (2006) evaluated the influence of factors such as vegetation, slope and sampling angle on the overall accuracy of a LiDAR (Light Detection And Ranging)-derived DEM. Kolecka and Kozak (2013) evaluated vertical accuracy of open source SRTM X-band DEM in a mountainous area (Polish Tatra Mountains) with respect to a high-resolution aerial photogrammetric DEM and found RMSE of 38.47 m in measurements. They observed that the presence of forest cover, local incidence angle, slope, aspect and radar beam geometry were the main factors affecting the accuracy of SRTM X-band DEM. They found out that the C-band DEM had better accuracy in most of the instances.

The present study evaluates freely available ASTER GDEM V2, SRTM X-band DEM and CartoDEM with respect to the high resolution (1 m) aerial photogrammetric DEM (ADS80 DEM) for parts of Himalayas. This high-resolution DEM was generated using digital aerial photogrammetric survey data of 40 cm Ground Sampling Distance (GSD), captured through airborne ADS80 push-broom camera for the first time in Indian Himalayan context. In an earlier attempt, Singh *et al.* (2014) assessed the vertical accuracy of this high-resolution DEM and observed high absolute vertical accuracy with RMSE of lesser than 1 m and linear error of 1.60 m at 90 % confidence interval (LE90). This high accuracy ADS80 DEM was resampled to 30 m spatial resolution for using it as the reference DEM. Elevation differences were obtained by subtracting the elevations of DEMs from the reference DEM and further used for the statistical analysis. A more detailed, accurate analysis was done

for different terrain scenarios (all possible combinations of different terrain parameters, e.g. slopes, aspect directions, elevation zones and land cover classes) consisting of various classes of aspect, slope, land cover and elevation of the study area. ASTER GDEM V2 was found to be the best representation of the terrain, followed by SRTM-X DEM and CartoDEM. The results are discussed, in detail, in Sect. 5 for the possible explanations.

2. Study Area

The study area (Fig. 1) lies in the NW-Himalaya, covering parts of Kullu and Lahaul and Spiti districts of Himachal Pradesh, India. The geographical extent of the study area is from 77°04′00″E/32°29′31″N to 77°16′46″E/32°13′43″N with the presence of high, rugged mountains, narrow valleys, and deep gorges consisting of very high slope gradient. The mean altitude of the area is 4431 m above MSL (mean sea level). This study area was selected because of the presence of the high accuracy aerial DEM as a reference for only this part of the Himalaya. In addition, this study area represents all the possible terrain classes in case of a complex mountainous terrain. Thus, this extent of the study area could be taken as a representative of the entire Himalayan terrain.

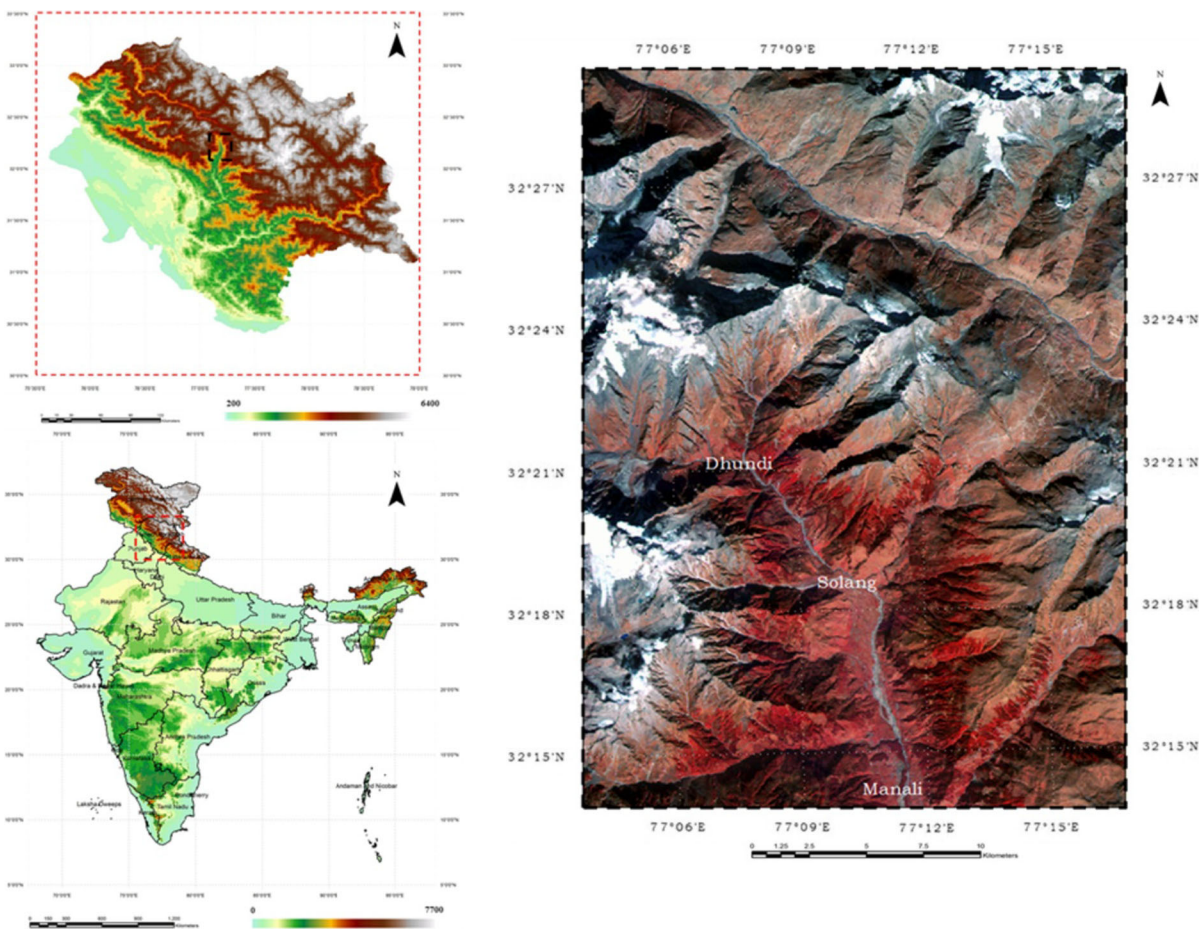

Figure 1
Study area (*right* Landsat 5 TM, 4-3-2 false colour composite image)

3. Materials and Methods

3.1. Data Used

3.1.1 ADS80 High Resolution DEM

The ADS80 high-resolution DEM at 1 m spatial resolution was generated by SASE (Snow and Avalanche Study Establishment) through photogrammetric processing of airborne ADS80 linear push broom sensor captured stereo images (Gupta *et al*. 2014). The ADS80 stereo images of 40 cm GSD were acquired in the month of February, 2011. Singh *et al.* (2014) tested the accuracy of this DEM with 20 DGPS (Differential global positioning system) points reported RMSE and standard deviation of 0.97 and 0.99 m, respectively, along with LE90 of 1.36 m.

3.1.2 ASTER GDEM V 2.0

Development of ASTER GDEM V2 was a collaborative effort of the Ministry of Economy, Trade, and Industry (METI), Japan and the National Aeronautics and Space Administration (NASA), United States of America (Robinson *et al*. 2014). The ASTER sensor was launched in December 1999 on-board NASA's Terra spacecraft with along-track stereoscopic capability (Hirano *et al*. 2003). The GDEM product is generated using automatic stereo correlation of millions of stereo pairs acquired through ASTER near infrared spectral band nadir-viewing (3N) and backward-viewing (3B) telescope (Mukherjee *et al*. 2013). ASTER GDEM is considered very useful for terrain research and application areas because of its free accessibility and global coverage (Schneevoigt *et al*. 2008). ASTER GDEM V2 is generated with a spatial resolution of about 30 m (1 arc-second) from the original 15 m ASTER image GSD in the horizontal plane (Arefi and Reinartz 2011). According to ASTER GDEM V2 validation report (Tachikawa *et al*. 2011), absolute vertical accuracy of the ASTER GDEM V2 (released on October 17, 2011) is 17 m LE95 (linear error at 95 % confidence) when compared to 18,000 geodetic control points. ASTER GDEM V2 was downloaded from http://gdem.ersdac.jspacesystems.or.jp.

3.1.3 SRTM X-Band DEM

SRTM X-band DEM was generated using X-band synthetic aperture radar (SAR) data (Czubski *et al*. 2013). The X-band data were acquired during the Shuttle Radar Topographic Mission, collaborated by the NASA/JPL (National Aeronautics and Space Administration/Jet Propulsion Laboratory, USA), the Italian Space Agency (Italian: Agenzia Spaziale Italiana; ASI), and the German Aerospace Center (DLR) in 2000 (Farr *et al*. 2007). With the objective to generate a global high-resolution DEM, two interferometric radar systems (C-band and X-band) on board the Space Shuttle Endeavour acquired data from February 11 to 22, 2000 (Sun *et al*. 2003). SRTM C-band DEM (3-arc-second, 90 m resolution) is freely available for the entire world and can be downloaded freely from the USGS website. The X-band data that cover approximately 58 million km^2 were processed by DLR (Rabus *et al*. 2003). The freely available SRTM X-band DEMs (covering entire globe between 60°N and 56°S) were generated through interferomeric processing of X-band SAR data acquired during SRTM mission (Hoffmann and Walter 2006). The coverage of the X-band DEM is not continuous because it covers approximately half of the area covered by C-band SAR sensor due to its narrower ground track (Kolecka and Kozak 2013). According to DLR SRTM X-SAR DEM readme file (https://centaurus.caf.dlr.de:8443/eoweb-ng/licenseAgreements/DLR_SRTM_Readme.pdf) provided with the data, absolute and relative vertical accuracy is ±16 of ±6 m, respectively, for 90 % of the data. SRTM X-band DEM was downloaded from EOWEB official web portal (https://centaurus.caf.dlr.de:8443/eoweb-ng/template/default/welcome/entryPage.vm).

3.1.4 CartoDEM

Cartosat-1 satellite was launched by the Indian Space Research Organization (ISRO) on May 5, 2005 (Martha *et al*. 2010). Cartosat-1 is equipped with in-orbit stereo capabilities, useful for DEM generation (Gianinetto 2009). The freely available 30 m spatial resolution Cartosat-1 DEM was downloaded from the NRSC website (http://www.bhuvan.nrsc.

gov.in). The operational procedure of CartoDEM generation comprised stereo strip triangulation of 500 × 27 km segment with 30 m posting (Muralikrishnan *et al*. 2013). Absolute vertical accuracy for CartoDEM for hilly area claimed by NRSC is 8 m (LE90) (Muralikrishnan *et al*. 2011).

3.1.5 Landsat 5 TM Image

A cloud-free Landsat 5 TM (Thematic Mapper) satellite image of 22 October, 2011, with 30 m spatial resolution, covering an area of 185 × 185 km^2 was downloaded from the USGS global visualization viewer (glovis.usgs.gov) to obtain land cover classes within the study area.

3.2. Methodology

Consideration of the terrain parameters individually is only a partial indicative of the vertical accuracy of DEMs. In the real earth scenario, different combinations of parameters exist and

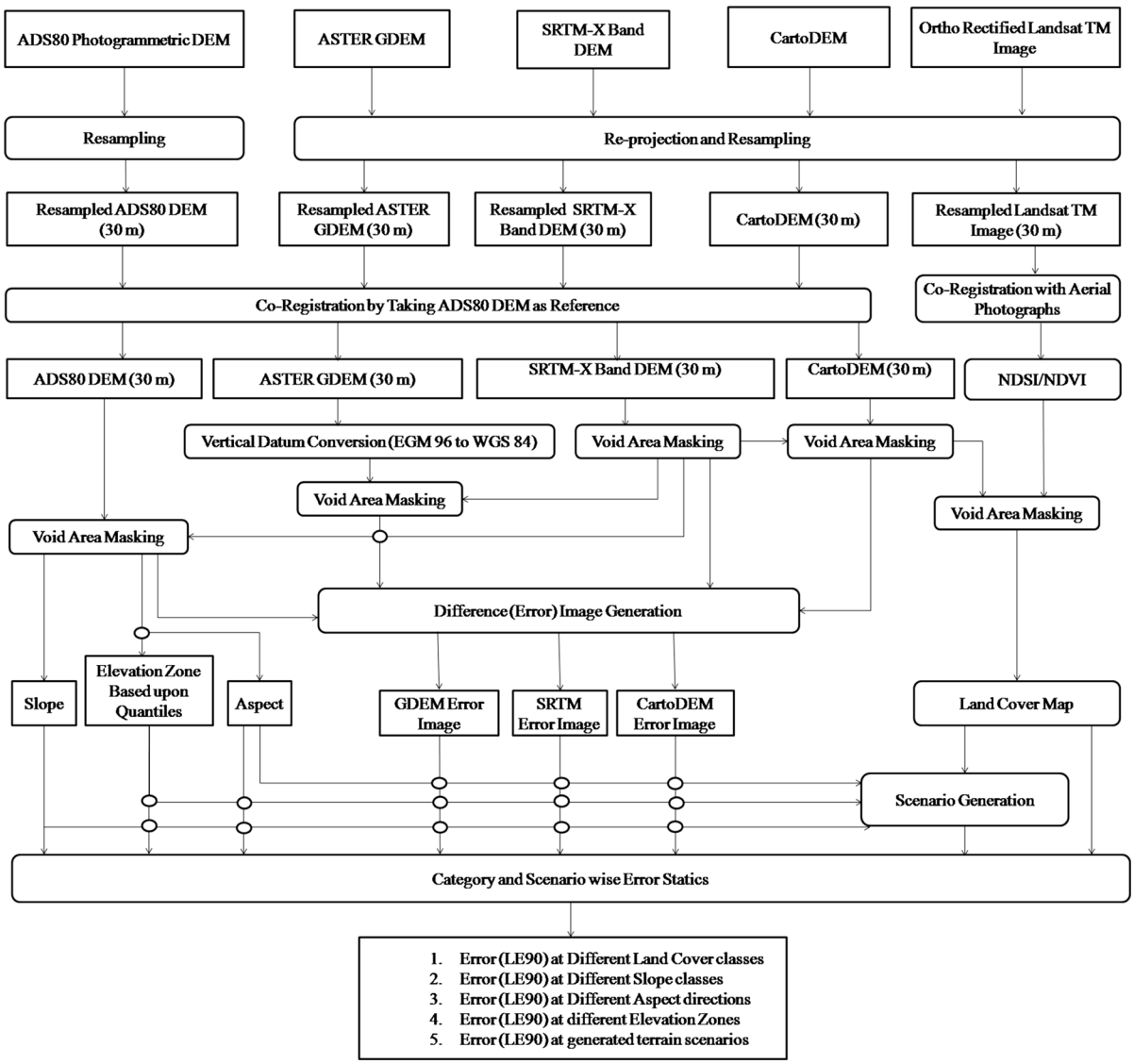

Figure 2
Methodology followed

considering the combined effect of all these conditions would give an actual estimate of the errors. Therefore, the proposed methodology (Fig. 2) presents a workflow for generation of such scenarios and accuracy assessment. Following paragraphs discuss the steps involved.

3.2.1 Projection, Pixel Size Matching and Co-Registration

ADS80 DEM was in UTM WGS84, Zone 43 N projection. All other data were re-projected to this projection system. The datasets were resampled using the nearest neighbour algorithm to a pixel size of 30 m for further processing.

The two DEMs are sensitive to misregistration for areas with significant relief as a shift of fraction of a pixel may cause significant changes in the elevation difference (Ni *et al*. 2014). The error caused by subpixel misregistration of the two DEMs was greater than or equal to the true difference between the two models (Niel *et al*. 2008). Precise co-registration of DEMs is difficult due to their continuous nature and very less tonal and textural variations in between the nearby pixels. Shaded-relief matching approach proposed by Aguilar *et al*. (2010b) is useful for the precise co-registration of DEMs. The Landsat image was co-registered with the aerial photographs. The error statistics for co-registration process is given in Table 1.

3.2.2 Vertical Datum Matching and Void Area Masking

The vertical datum of various elevation datasets used in the study differs (Table 2). To conduct a consistent comparison among the two height data sets, heights must refer to the same vertical datum (Baghdadi *et al*. 2011). As evident in Table 2, all the DEMs except ASTER GDEM V2 were in WGS84 datum. Therefore, to bring uniformity for further analysis, EGM96 geoid datum of ASTER GDEM V2 was converted to WGS84 using Eq. 1 given in Mukherjee *et al*. (2013):

$$E = H + G \tag{1}$$

Equation 1 represents the geoid separation/geoid undulation (G), the ellipsoid height (E) and the height above the geoid surface/orthometric height (H).

For fair comparison and analysis purpose, voids in (29.89 % of total area) SRTM X-band DEM (Fig. 3a)

Table 1

Error statistics for co-registration

S. No.	Data type	Observed RMSE in X direction after co-registration in ground units (m)	Observed RMSE in Y direction after co-registration in ground units (m)	Observed RMSE (m)
1	ADS80 DEM	Master DEM		
2	ASTER GDEM	1.06	5.54	5.64
3	SRTM-X Band DEM	6.90	4.34	8.15
4	CartoDEM	8.50	11.73	14.49
5	Landsat 5 TM	9.53 (with respect to aerial photographs)	3.23 (with respect to aerial photographs)	10.06

Table 2

Datum information of used DEMs

S. No.	DEM	Provider	Projection/datum	Vertical datum	Spatial resolution	% Coverage of study area
1	ADS80	SASE	UTM 43/WGS84	WGS84	1 m	100
2	ASTER GDEM V2.0	METI and NASA	Geographic (Lat/Long)/WGS84	EGM96	1 arc second	100
3	SRTM-X Band DEM	DLR	Geographic (Lat/Long)/WGS84	WGS84	1 arc second	70
4	CartoDEM	NRSC	Geographic (Lat/Long)/WGS84	WGS84	1 arc second	100

Source: ASTER and CartoDEM handbooks, SRTM-X 'Read me' file

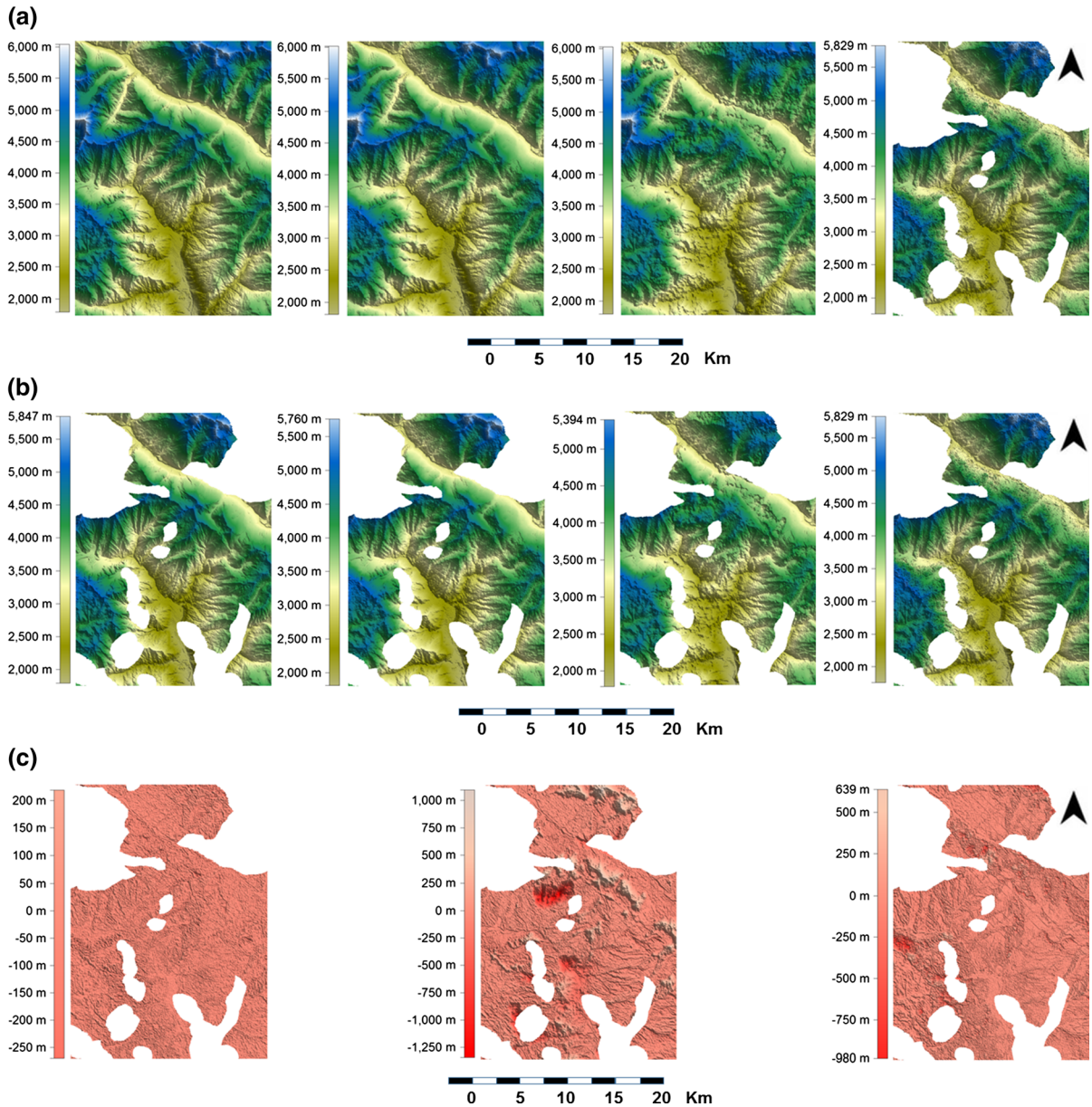

Figure 3
a DEMs: *left to right* ADS80, ASTER GDEM, CartoDEM, SRTM X band DEM; **b** void masked DEMs: *left to right* ADS80, ASTER GDEM, CartoDEM, SRTM X band DEM; **c** elevation difference images with respect to ADS80 DEM: *left to right* ASTER GDEM, CartoDEM, SRTM X band DEM

were masked out and the same masks were applied to other DEMs used in this study. Figure 3b shows all three DEMs after applying the void mask. Table 3 presents the statistics for the resampled 30 m DEMs used in this study before and after applying void mask.

3.2.3 *Derivation of Terrain Attributes, Difference Images and Land Cover Classes*

The parameters derived from ADS80 DEM were slope (Fig. 4a), aspect (Fig. 4b) and elevation zones (Fig. 4c). These were taken as real terrain conditions

Table 3

Statistical summary of used DEMs

Used DEMs	Before void mask					After void mask				
	Number of Pixels	Mean (m)	Median (m)	Min (m)	Max (m)	Number of Pixels	Mean (m)	Median (m)	Min (m)	Max (m)
ADS80	659,520	3760	3784	1791	6039	462,364	3718	3756	1791	5847
GDEM	659,520	3788	3813	1812	6013	462,364	3717	3759	1784	5735
CartoDEM	659,520	3740	3773	1791	6027	462,364	3697	3748	1791	5394
SRTM-X DEM	659,520	−380	3278	−9999	5829	462,364	3721	3763	1758	5829

and hence the reference because of very high accuracy of the DEM. Jones (1998) reported four-cell method as the most accurate one for calculating slope and aspect directions. This method had been adopted for generating slope and aspect in the present study. Four-cell method considers two orthogonal components (in x and y directions) of slope. Corresponding aspects were computed for these slopes. The DEM was reclassified into five elevation zones based on the quantiles. Also, the difference images (Fig. 3c) for statistical analyses were generated for freely available DEMs by subtracting them from ADS80 DEM.

Indices (NDSI—Normalized Difference Snow Index, NDVI—Normalized Difference Vegetation Index) based classification was performed on the Landsat 5 TM image to demarcate four land cover classes, i.e., barren land/exposed rocks, shrubs, forest, snow and/or ice (Fig. 4d).

3.2.4 Scenario and Statistics Generation

Terrain scenarios were generated using different combinations of terrain parameters. Intersection operation was performed between all the layers of importance and statistics was generated for each scenario having at least one representative pixel. Finally, LE90 was computed. LE90 represents the linear vertical distance between 90 % of reference points and their respective twin matching counterparts acquired in an independent survey. LE90 is the 90th percentile linear error, i.e., minimum of 90 % of vertical errors falls within the stated LE90 value. In case the vertical error is normally distributed, the factor 1.6449 is multiplied with RMSE to compute vertical accuracy at the 90 % confidence level (Greenwalt and Shultz 1968). But in our case, the errors were not normally distributed as evident from the skewness and kurtosis values in Table 4. Therefore, we reported the LE90 by manual sorting of linear errors.

4. Results

4.1. Visual Comparison and Statistical Summary of Used DEMs

A visual comparison between the DEMs can be easily made by looking at Figs. 3a and 5. It is perceivable that ASTER GDEM V2 most closely matches with the ADS80 DEM at higher elevations. The reference ADS80 DEM has very smooth appearance in which, ridges and gullies look very sharp, and are easily identifiable. Also, all the major and minor drainage lines are visible. ASTER GDEM V2 in terms of visual quality appears to be a coarser version of the ADS80 DEM in which ridges (B1 part in Fig. 5) and gullies are identifiable. The ridges are better distinguished in ADS80 (B) and SRTM X-band DEM (B3 part) than in B1 and B2. Part of valley in ADS80 (C) and SRTM X-band DEM (C3) is better represented than C1 and C2. The inherent spikes in ASTER GDEM V2 can be clearly seen in the form of small rough patches (compare A1 part with A in Fig. 5). A2 represents the inherent mosaicing error in CartoDEM. Y represents the voids in SRTM-X DEM. Another very interesting observation is shown with dashed polygons on SRTM X-band DEM in Fig. 5. It is evident that all the inherent spikes (noise) are on North-East, East and South-East facing slopes.

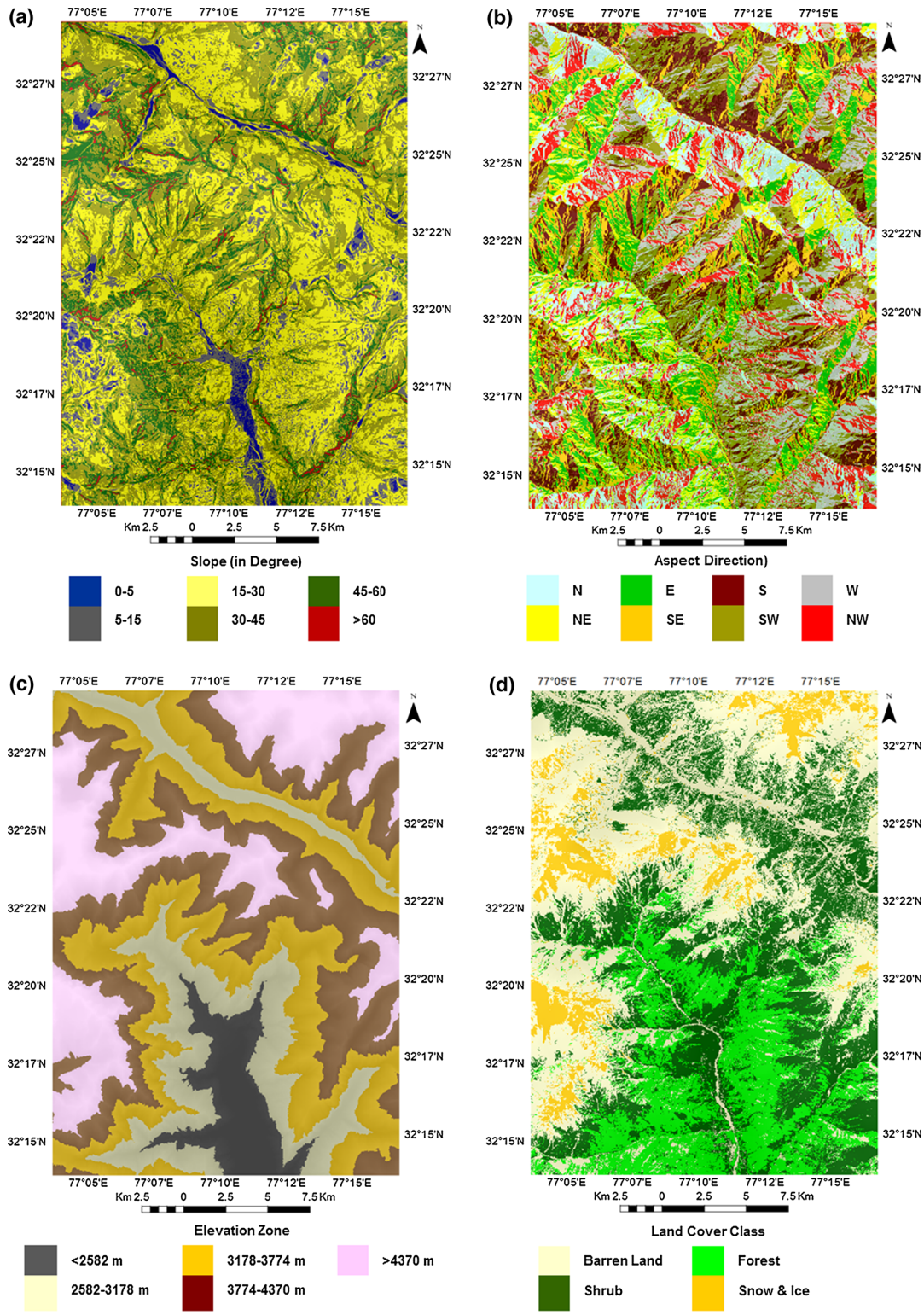

Figure 4
a Slope, **b** aspect, **c** elevation zones and land cover using Landsat 5 TM image

Table 4
Statistical summary of error DEMs

ADS80-"DEM"	*N*	Mean (m)	Median (m)	Min (m)	Max (m)	*Q* (25 %) (m)	*Q* (75 %) (m)	Range (m)	*Q* range (m)	SD (m)	SE (m)	Skewness (m)	Kurtosis (m)	RMSE (m)	LE90 (m)
GDEM	462,364	0.75	−0.97	−242.23	248	−11.83	11.40	490	23.23	23.86	0.03	0.49	6.27	23.87	36.25
SRTM-X DEM	462,364	−3.29	3.32	−979.95	639	−13.64	18.69	1619	32.33	73.29	0.11	−3.27	27.05	73.36	75.20
CartoDEM	462,364	20.37	10.65	−1335.2	1096	−22.76	43.84	2431	66.60	165.17	0.24	−0.41	10.12	166.42	256.38

N number of pixels, *Q* quartile

Numerous numbers of these spikes are also an explanation for the distinct peaks in the histogram of SRTM X-band DEM (Fig. 6).

4.2. Statistical Summary of Error DEMs

Table 4 and quantile–quantile (*Q*–*Q*) plot represented in Fig. 7 are representative of statistical summaries of the difference/error DEMs. Least differences in elevation were shown by ASTER GDEM V2, whereas the CartoDEM varied widely from ADS80 DEM. Subsequently, ASTER GDEM V2 showed lower standard deviation (23.86 m) and RMSE (23.87 m). Given below are the statistical observations of error DEMs with respect to different terrain conditions (Fig. 8).

4.2.1 Slope Wise Statistical Summary of Error DEMs

Table 5 shows the statistical parameters derived to comment upon the accuracy of the DEMs in different classes of slope. All the DEMs showed overall increasing LE90 with increasing slope. ASTER GDEM V2 gave better accuracy at all the slopes and increase in LE90 was nearly constant. As given in Fig. 8, there was a steep increase in LE90 observed between 30° and 60° slopes in SRTM X-band DEM. CartoDEM showed a decreasing trend for LE90 till 30° slopes, but a sharp increase beyond that. Figure 9 shows *Q*–*Q* plot of elevation differences of ASTER GDEM V2, SRTM X-band DEM and CartoDEM, respectively, for various classes of slope with respect to ADS80 DEM. As mentioned in Table 5, slope class 3 (15°–30°) contains highest numbers of pixels with LE90 of 26.55, 44.47, and 161.60 m for ASTER GDEM V2, SRTM-X DEM and CartoDEM, respectively.

4.2.2 Aspect Wise Statistical Summary of Error DEMs

Table 6 gives an idea about the accuracy of DEMs in different classes of aspect. ASTER GDEM V2 gave consistency in accuracy in all the classes of aspect with LE90 within the range of 27–47 m (Fig. 8; Table 6). SRTM X-band DEM showed more variation with LE90 varying from 28 to 202 m

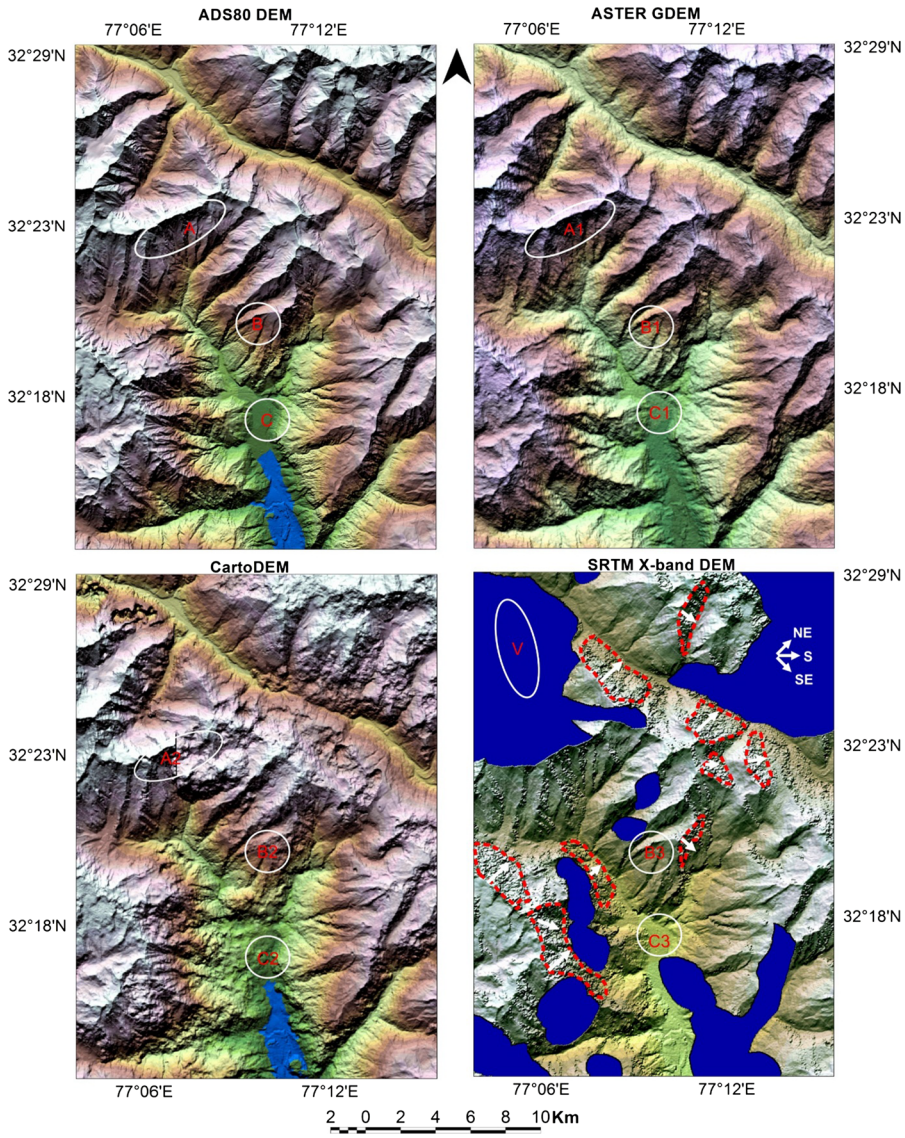

Figure 5
Painted relief images of DEMs (*B*, *B1*, *B2*, and *B3* ridges and gullies; *C*, *C1*, *C2*, *C3* valley; compare *A1* with *A* for observing inherent spikes in the ASTER GDEM V2; *V* voids in the SRTM X-band DEM, *A2* mosaicing error in the CartoDEM). *Dashed polygons* on the SRTM X-band DEM show inherent spikes on North-East to South-East facing slopes

(Fig. 8; Table 6). SRTM X-band DEM showed a particular trend from North-East to South-East aspects as the accuracy improved significantly (Fig. 8). CartoDEM gave poorest accuracy for all the aspect classes (Fig. 8). Figure 10 shows *Q*–*Q* plot of elevation differences of ASTER GDEM V2, SRTM X-band DEM and CartoDEM, respectively, for various classes of aspect with respect to ADS80 DEM. For all the DEMs, the highest number of pixels is represented by aspect classes 6 (SW) and 7 (W).

4.2.3 *Elevation Zone Wise Statistical Summary of Error DEMs*

Table 7 tells about the accuracy of the DEMs in different classes of the elevation zones. ASTER GDEM V2 gave consistency in accuracy in all the

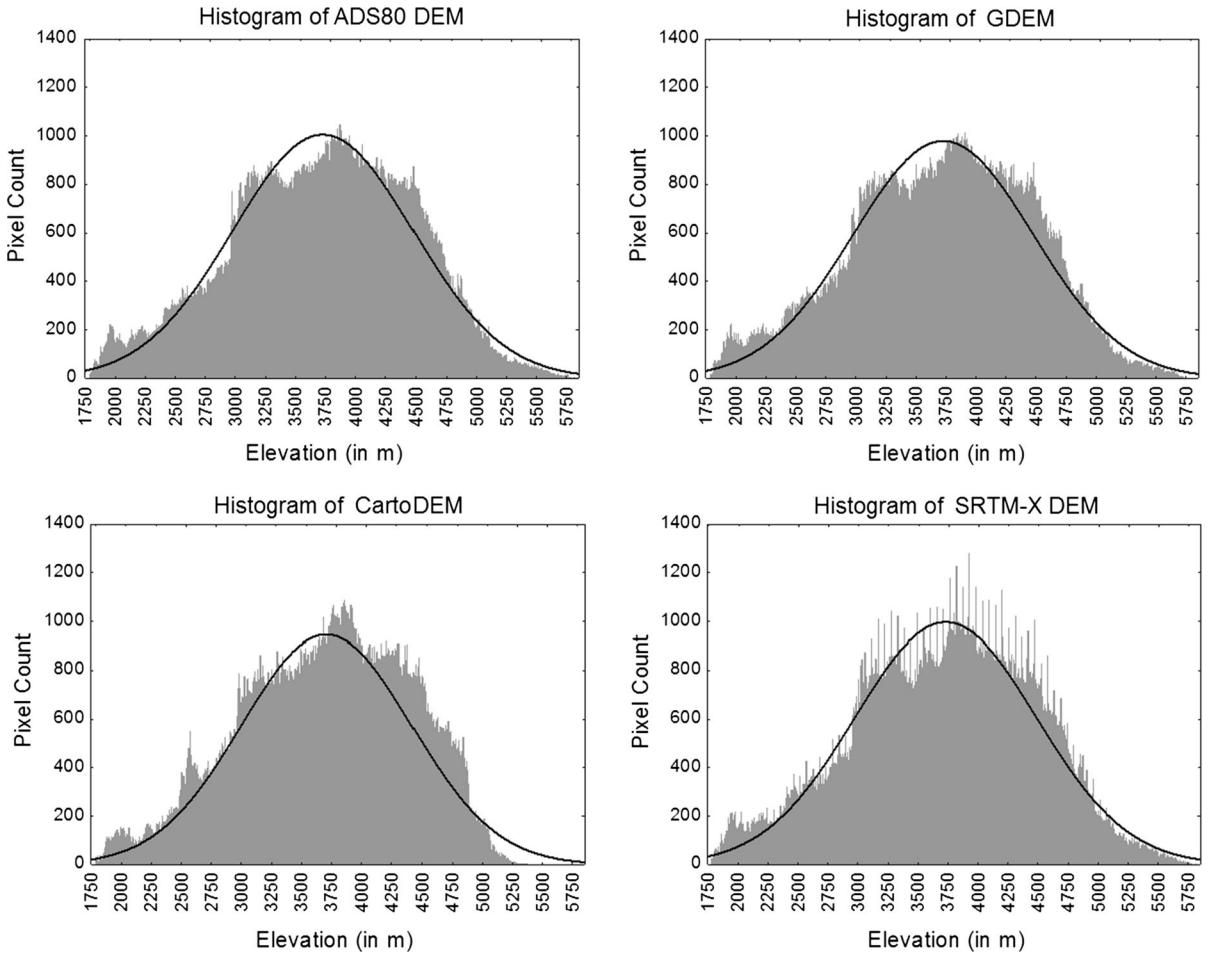

Figure 6
Histograms of different DEMs. *X* axis shows elevation in meter

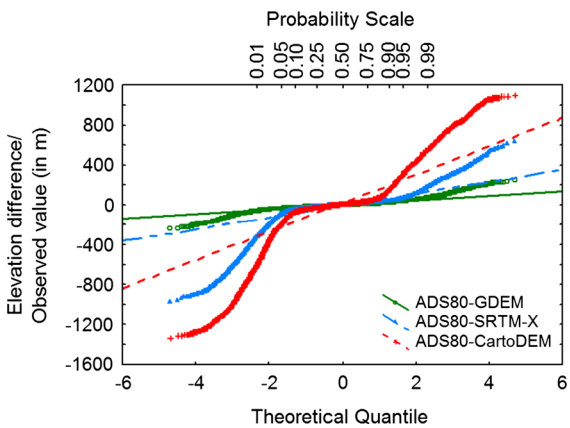

Figure 7
Quantil–quantile plot of difference images. *Y* axis shows difference in elevation in meter with respect to the ADS80 DEM

elevation zones with LE90 within the range of 28–48 m (Fig. 8; Table 7). From the 4th elevation zone onwards, there was a sudden linear increasing trend in LE90 (Fig. 8) in case of ASTER GDEM V2. But the interesting thing to observe was that linearly increasing LE90 of SRTM X-band DEM stabilized and became almost constant beyond the 4th elevation zone (Fig. 8). CartoDEM again showed poorest accuracy with fluctuating trend for LE90. Figure 11 shows *Q*–*Q* plots of elevation differences of ASTER GDEM V2, SRTM X-band DEM and CartoDEM, respectively, for various classes of elevation with respect to ADS80 DEM. For all the DEMs, the highest numbers of pixels is represented by elevation classes 3 and 4.

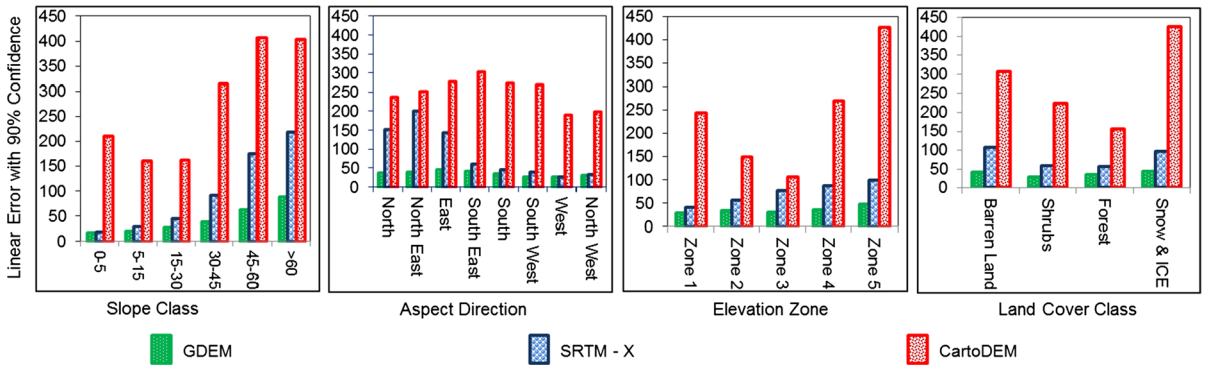

Figure 8
LE90 (linear error with 90 % confidence) in meter observed for various terrain classes of slope, aspect, elevation zones and land cover (elevation zones: 1 = ≤2581.76 m, 2 = 2581.76–3177.79 m, 3 = 3177.79–3773.83 m, 4 = 3773.83–4369.86 m, 5 = ≥4369.86 m)

Table 5

Slope wise statistical summary of error DEMs

Slope class	Valid *N*	ADS80-GDEM (m)				ADS80-SRTM-X DEM (m)				ADS80-CartoDEM (m)			
		Mean	SD	RMSE	LE90	Mean	SD	RMSE	LE90	Mean	SD	RMSE	LE90
1	11,066	−0.94	11.72	11.75	17.34	5.02	27.57	28.03	19.71	−39.2	116.36	122.78	209.83
2	47,661	−2	13.7	13.84	21.03	2.35	40.54	40.61	28.21	−9.18	114.26	114.62	161.03
3	183,532	−1.1	17.02	17.06	26.55	0.6	49.09	49.09	44.47	8.11	130.31	130.56	161.6
4	165,350	1.8	24.99	25.06	39.22	−5.67	81.51	81.71	91.45	32.9	184.96	187.87	315.57
5	47,690	6.04	39.37	39.83	63.19	−14.91	121.72	122.63	175.3	60.17	227.67	235.49	406.57
6	7065	9.71	52.25	53.14	88.65	−21.56	138.03	139.7	217.87	68.78	229.09	239.17	403.62

Slope class 1 = ≤5°, 2 = 5°–15°, 3 = 15°–30°, 4 = 30°–45°, 5 = 45°–60°, 6 = >60°

4.2.4 *Land Cover Wise Statistical Summary of Error DEMs*

Table 8 tells about the accuracy of the DEMs in different land cover classes. Among all DEMs, ASTER GDEM V2 gave better accuracy with minimum LE90 of 29 m for shrubs and maximum LE 90 of 43 m for snow and ice class (Fig. 8; Table 8). All DEMs gave their best accuracies in shrubs and forest classes and their worst in snow/ice and barren classes (Fig. 8). Figure 12 shows *Q*–*Q* plots of elevation differences of ASTER GDEM V2, SRTM X-band DEM and CartoDEM, respectively, for various classes of land cover with respect to ADS80 DEM. For all the DEMs, the highest number of pixels is represented by elevation classes 1 (barren and exposed rocks) and 2 (shrubs).

4.3. *Error Estimation for Various Terrain Scenarios*

The analyses discussed above are accounting for one terrain condition at a time. But in the real earth scenario, all these conditions co-exist and their combinations decide the final accuracies of DEMs. In the real world where the slopes exist not in isolation, but they have some aspects also along with particular elevations and land covers. Thus, talking about the errors in any one of these terrain characteristics in isolation is not realistic and a combination of these all can give a real estimate. To the best of our knowledge, this is the first of such attempt to describe accuracies of DEMs based on combinations of different terrain conditions in the high mountains. Figures 13 and 14 show mean error and the LE90, respectively, for various terrain scenarios. It is clearly evident that ASTER GDEM V2 is giving the best

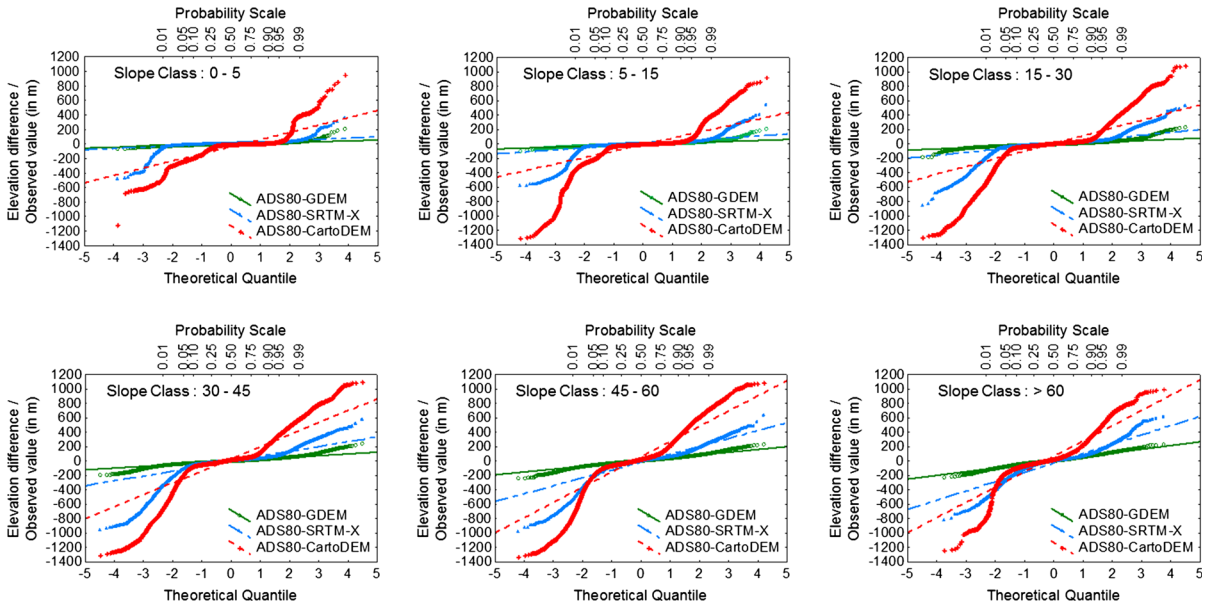

Figure 9
Quantile–quantile plot of elevation difference of different DEMs with respect to the ADS80 DEM for various slope classes. *Y* axis shows difference in elevation in meter with respect to the ADS80 DEM

Table 6

Aspect wise statistical summary of error DEMs

Aspect class	Valid *N*	ADS80-GDEM (m)				ADS80-SRTM-X DEM (m)				ADS80-CartoDEM (m)			
		Mean	SD	RMSE	LE90	Mean	SD	RMSE	LE90	Mean	SD	RMSE	LE90
1	46,719	−7.06	25.12	26.09	39.20	−14.33	109.63	110.57	153.99	11.38	145.55	146.00	237.27
2	52,092	−2.26	27.85	27.95	40.49	−17.40	129.77	130.93	202.18	15.67	152.85	153.66	253.09
3	45,630	11.74	27.62	30.02	47.85	2.90	102.90	102.94	145.65	14.89	172.75	173.39	279.18
4	55,892	12.77	24.39	27.53	43.14	8.81	55.20	55.90	62.34	22.58	189.29	190.63	303.66
5	64,902	7.40	22.25	23.45	36.42	1.16	38.20	38.22	47.61	35.28	175.32	178.83	275.00
6	74,649	0.33	18.25	18.26	27.99	−3.90	27.78	28.05	40.96	31.83	168.98	171.95	270.28
7	66,588	−6.96	16.54	17.94	27.72	−2.58	26.56	26.69	28.34	17.99	154.92	155.96	192.63
8	55,892	−8.88	19.45	21.34	33.36	−3.29	54.29	54.39	35.59	4.70	150.95	151.02	201.16

Aspect 1 = N, 2 = NE, 3 = E, 4 = SE, 5 = S, 6 = SW, 7 = W, 8 = NW

accuracies at all the combinations followed by SRTM X-band DEM. CartoDEM is widely in disagreement with all the DEMs in terms of elevation. The error in CartoDEM is typically higher at many terrain condition combinations.

In case of ASTER GDEM V2, forested, north facing (0°–5°) slopes falling under the 4th elevation zone showed minimum LE90 of 0.99 m. On the contrary, barren or exposed rocks with East facing (>60°) slopes falling under the 2nd elevation zone showed maximum LE90 of 166 m. For SRTM X-band DEM, the pixels with South-East facing slopes of 0°–5° falling under the 4th elevation zone covered with forests showed least LE90 of 0.33 m while maximum LE90 of 521 m was observed in the barren area with >60° North-East facing slope in the 4th elevation zone. In case of CartoDEM, the snow and/or ice pixels falling between 2581 and 3177 m elevation range with South-East facing slopes of 5°–15° showed least LE90 of 0.71 m while maximum

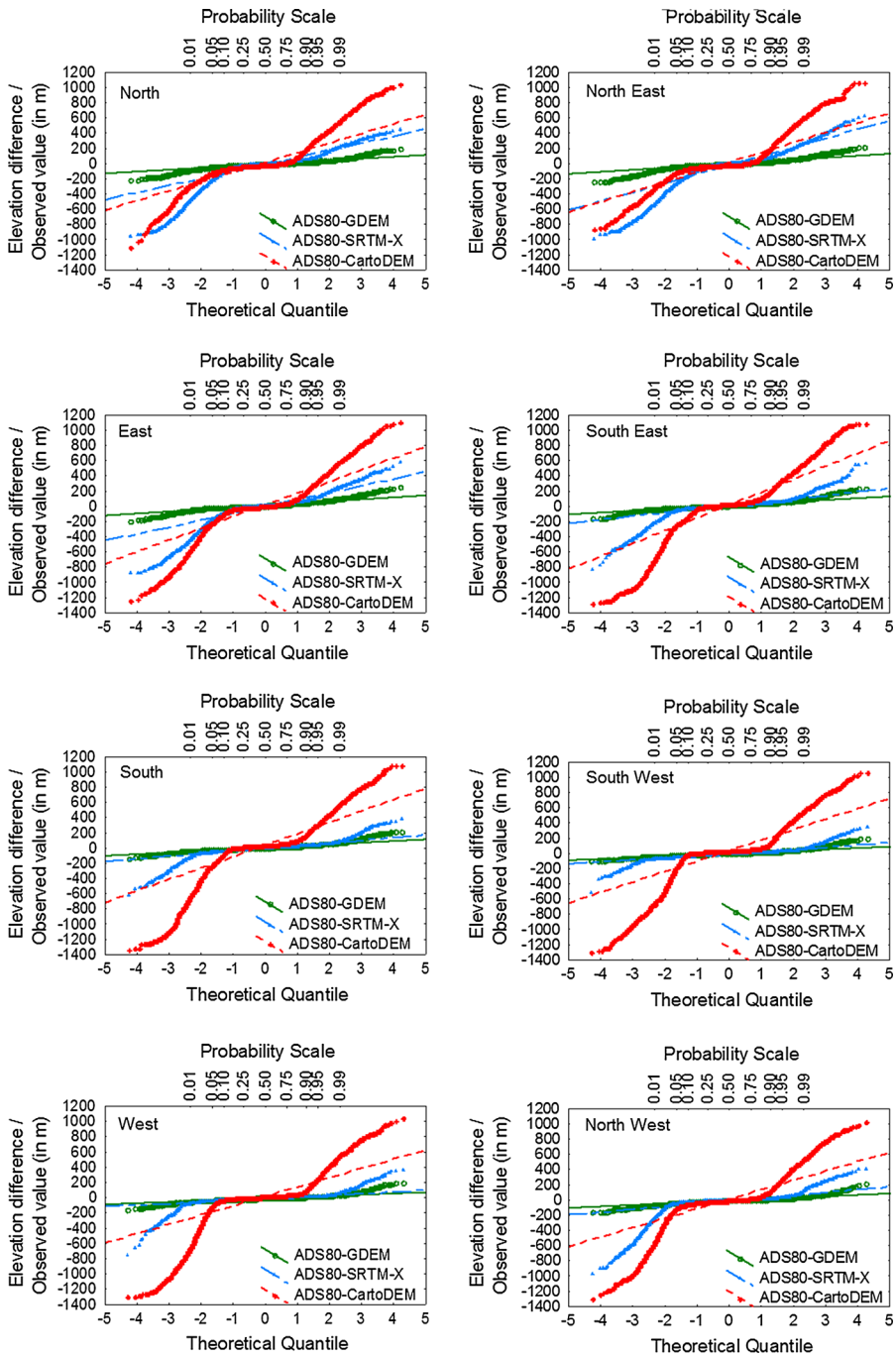

Figure 10
Quantile–quantile plot of elevation difference of different DEMs with respect to the ADS80 DEM for various Aspect directions. *Y* axis shows difference in elevation in meter with respect to the ADS80 DEM

Table 7

Elevation zone wise statistical summary of error DEMs

Elevation zone	Valid *N*	ADS80-GDEM (m)				ADS80-SRTM-X DEM (m)				ADS80-CartoDEM (m)			
		Mean	SD	RMSE	LE90	Mean	SD	RMSE	LE90	Mean	SD	RMSE	LE90
1	35,840	2.17	17.38	17.52	28.12	10.02	30.00	31.63	41.27	−89.31	126.05	154.48	244.05
2	76,094	2.96	21.55	21.75	34.22	4.79	48.33	48.57	56.09	3.68	99.88	99.95	149.37
3	123,301	−1.48	20.87	20.93	30.87	−4.87	71.23	71.40	75.97	−19.19	158.86	160.01	105.22
4	130,355	−1.27	23.18	23.21	34.60	−6.92	85.77	86.05	86.91	22.03	152.59	154.17	269.55
5	96,774	4.05	30.62	30.88	48.01	−7.70	83.44	83.80	98.73	122.26	189.86	225.82	425.44

Elevation zone (in m) 1 = ≤2582, 2 = 2582–3178, 3 = 3178–3774, 4 = 3774–4370, 5 = >4370

LE90 of 1266 m was observed for the snow and/or ice pixels in the 3rd elevation zone within the South facing slope of 45°–60°.

5. Discussion

A detailed visual comparison of the DEMs showed that CartoDEM described major hydrological features on the lower reaches in a clearer way than ASTER GDEM V2 and SRTM X-band DEM. This may be attributed to the observation that CartoDEM represented the lower elevations better than ASTER GDEM V2 and SRTM X-band DEM. On the other hand, CartoDEM was a poorer representative of higher elevations and ridge lines. Owing to this, the mean elevation of CartoDEM was also very different from reference DEM. In slope wise statistical summary of error DEMs (Table 5), CartoDEM showed a decreasing trend for LE90 till 30° slopes but the accuracy decreased sharply beyond that. This again proves that CartoDEM is able to capture flat valley portions in a better way than steeper higher slopes.

Slope wise statistical summary of error DEMs (Table 5) showed a sudden increase in LE90 between 30° and 60° slopes for SRTM X-band DEM. This may be attributed to 'side looking' way of data acquisition making these slopes particularly susceptible to vertical errors. This may also be a possible explanation for improved accuracy of SRTM X-band DEM specifically from the North-East to the South-East aspects. The elevation zone wise statistical summary of error DEMs (Table 7) showed a consistent performance by SRTM X-band beyond 4000 m elevation.

Land cover wise statistical summary of error DEMs (Table 8) showed that all DEMs gave their best accuracies in shrubs and forest classes and their worst in snow/ice and barren classes (Fig. 8). This may be attributed to the fact that source data acquisition times for all the DEMs were different. Vegetation cover is generally detectable in all the source data because it can come over snow cover beneath, but barren and snow covered parts are highly variable in the temporal domain.

The combination of terrain scenarios was thought as a better representative of the DEM errors as it simulated the real earth scenarios. In case of the error estimation for various terrain scenarios, error in CartoDEM was found to be typically higher in most cases. Despite the fact that both, ASTER GDEM V2 and CartoDEM are photogrammetrically derived DEMs, one of them showed better accuracy (ASTER GDEM V2) than that of the other (CartoDEM). Certainly, the methods of DEM generation and interpolation seem to be possible causes of this difference in accuracy. The inherent reasons behind such performance of the freely available CartoDEM, despite better spatial resolution of the source data, need a proper investigation though.

Li *et al.* (2013) reported 26 m (RMSE) absolute vertical accuracy for ASTER GDEM V2 by comparing high-accuracy GPS benchmarks elevation values with ASTER GDEM V2 at five study sites in China. In the present study also, the reported RMSE for ASTER GDEM V2 is approximately 24 m (Table 4). During the quality assessment and validation of SRTM X-band DEM based on the trigonometric points and reference DTM for a test site in south of Hannover (Germany), Koch *et al.*

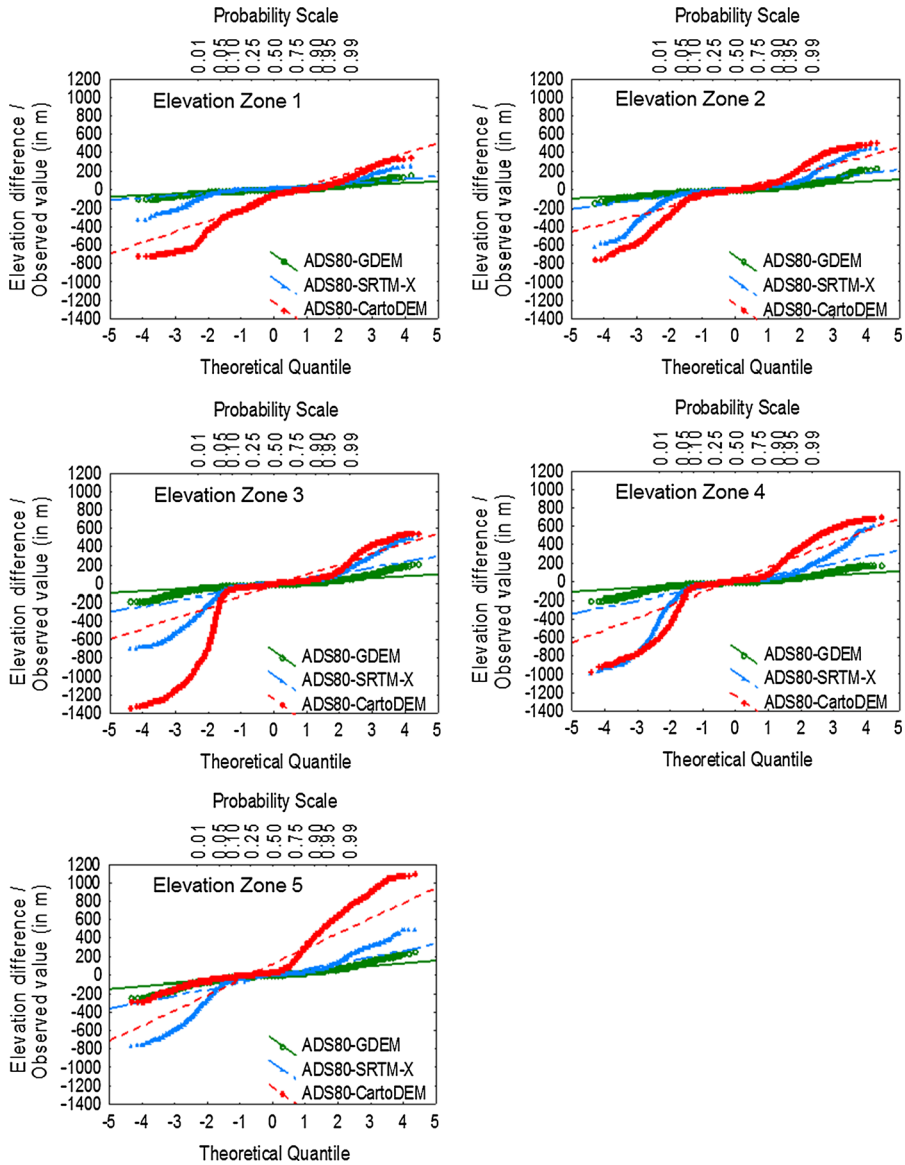

Figure 11

Quantile–quantile plot of elevation difference of different DEMs with respect to the ADS80 DEM for various elevation classes (zones). *Y* axis shows difference in elevation in meter with respect to the ADS80 DEM. Class description: elevation zone 1 = ≤2581.761, elevation zone 2 = 2581.761–3177.796, elevation zone 3 = 3177.795633–3773.829, elevation zone 4 = 3773.829928–4369.864, elevation zone 5 = >4369.864

(2002) observed maximum height difference of about 450 m in this area. Again, this maximum elevation difference is supported by the present study (Table 4) with a slight increase in height difference (189 m) due to the complexities of the Himalayan terrain. Till now, only one study (Muralikrishnan *et al*. 2013) performed a multi-approach evaluation of CartoDEM with respect to the ground control points, the relative difference between SRTM, ASTER DEMs and the ICESat (Ice, Cloud, and land Elevation Satellite) GLAS (Geoscience Laser Altimeter System) elevation values. The reported absolute height accuracy in hilly areas was 7 m vertical and 14 m horizontal accuracy. With respect to the SRTM over Indian

Table 8

Land cover wise statistical summary of error DEMs

Land cover class	Valid *N*	ADS80-GDEM (m)				ADS80-SRTM-X DEM (m)				ADS80-CartoDEM (m)			
		Mean	SD	RMSE	LE90	Mean	SD	RMSE	LE90	Mean	SD	RMSE	LE90
1	183,899	−0.95	26.88	26.90	41.30	−12.90	93.46	94.34	105.46	35.63	180.70	184.18	306.19
2	152,853	0.36	19.23	19.23	28.85	4.01	52.12	52.27	57.68	1.04	152.00	152.00	223.40
3	93,440	3.58	22.21	22.49	35.18	4.82	51.74	51.96	55.95	−7.92	117.18	117.45	154.93
4	32,172	4.07	28.50	28.79	43.04	−6.66	74.88	75.17	96.33	107.05	207.00	233.04	424.43

Land cover class 1 = barren land/exposed rock, 2 = shrubs, 3 = forest, 4 = snow and ice

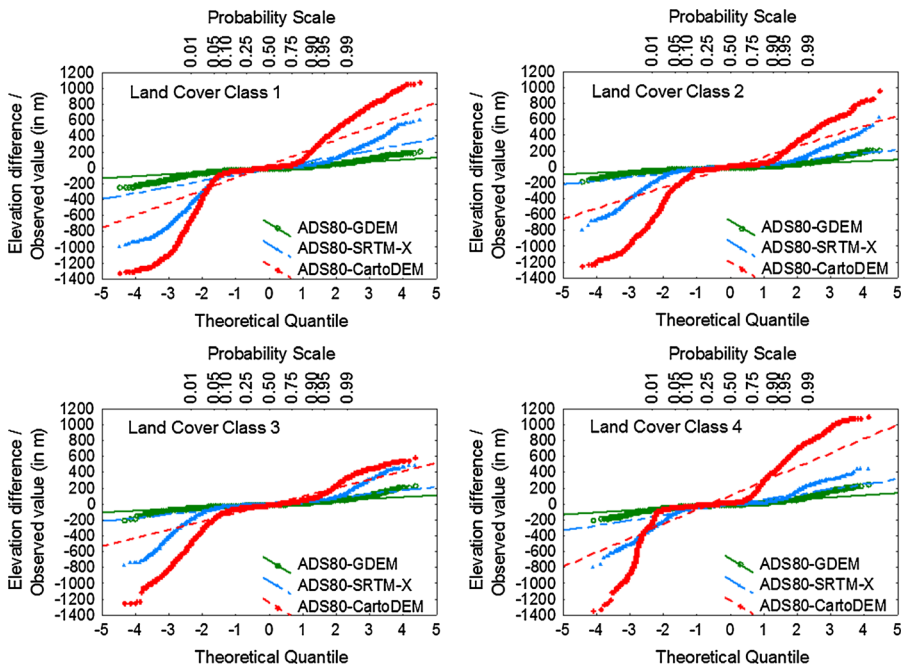

Figure 12

Quantile–quantile plot of elevation difference of different DEMs with respect to the ADS80 DEM for various land cover classes. *Y* axis shows difference in elevation in meter with respect to the ADS80 DEM. Class description: land cover class 1 = barren land/exposed rock, land cover class 2 = shrubs, land cover class 3 = forest, land cover class 4 = snow and ice

landmass, 90 % of the pixels reported were in range of ±8 m difference. Contrary to the Muralikrishnan *et al.* (2013) study, in the present study, CartoDEM was found to be performing worst for Himalayan terrain (Table 4).

6. Conclusions

This is the first study to look into real earth scenarios which affect the accuracy of generated DEMs in the complex terrains like Himalayan Mountain systems. The sources, base data and methodologies adopted in generating the DEMs taken for the study vary widely. Taking terrain parameters individually is only partially indicative of the vertical accuracy of

Figure 13 ▶

Mean error for various terrain scenarios. *Y* axis represents the mean error (elevation difference with respect to the ADS80 DEM) in meter. On *X* axis, the four numbers in each code represent class number for land cover, aspect, slope and elevation, respectively. In *Y* axis, the maximum and minimum values are fixed to 250 and −250, respectively, for enhancing the visibility. Values written in *red colour* for the CartoDEM) and in *blue colour* for the SRTM-X DEM represent terrain scenarios where values are crossing the fixed range of −250 to 250

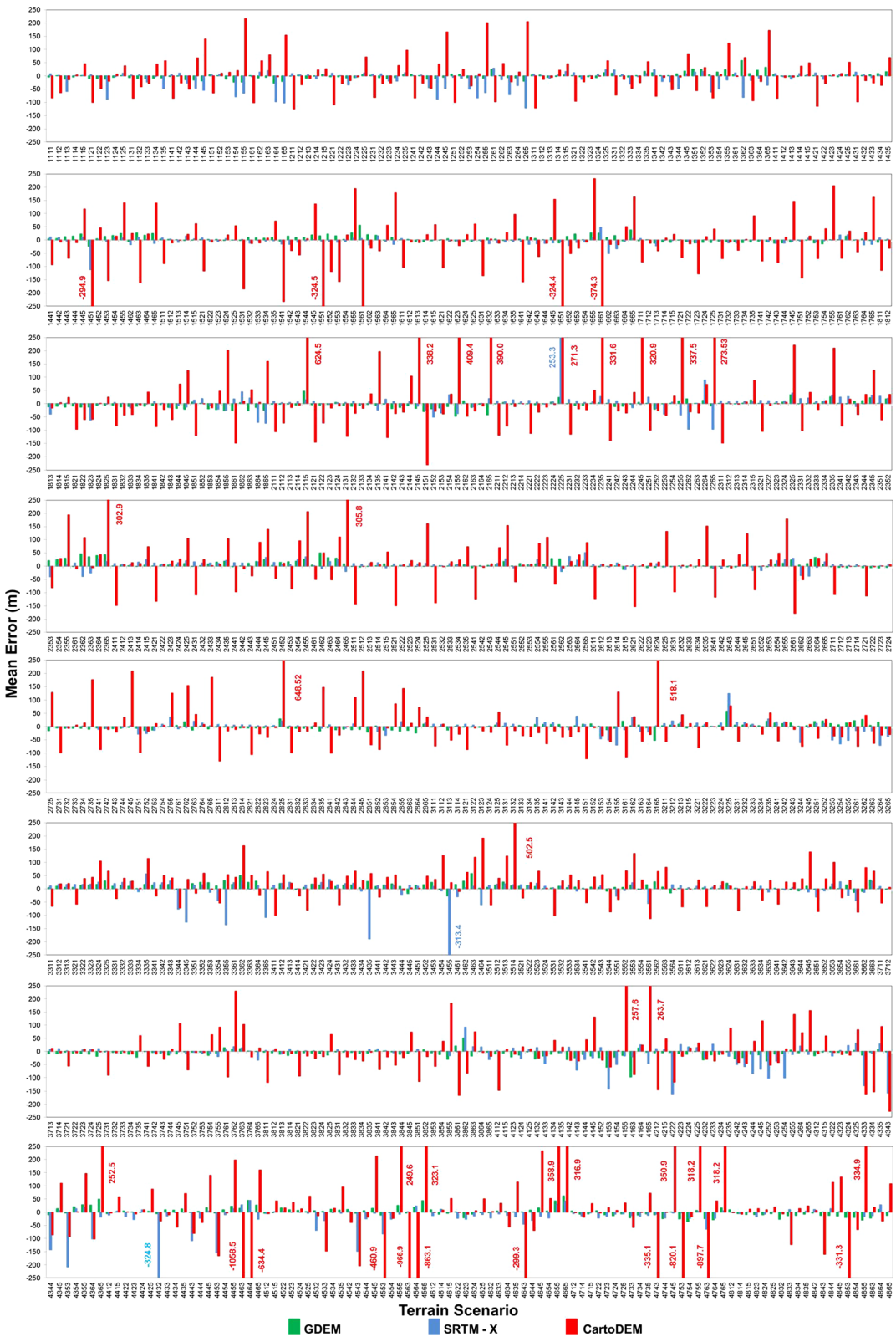
Mean Error (m)
Terrain Scenario
GDEM
SRTM - X
CartoDEM

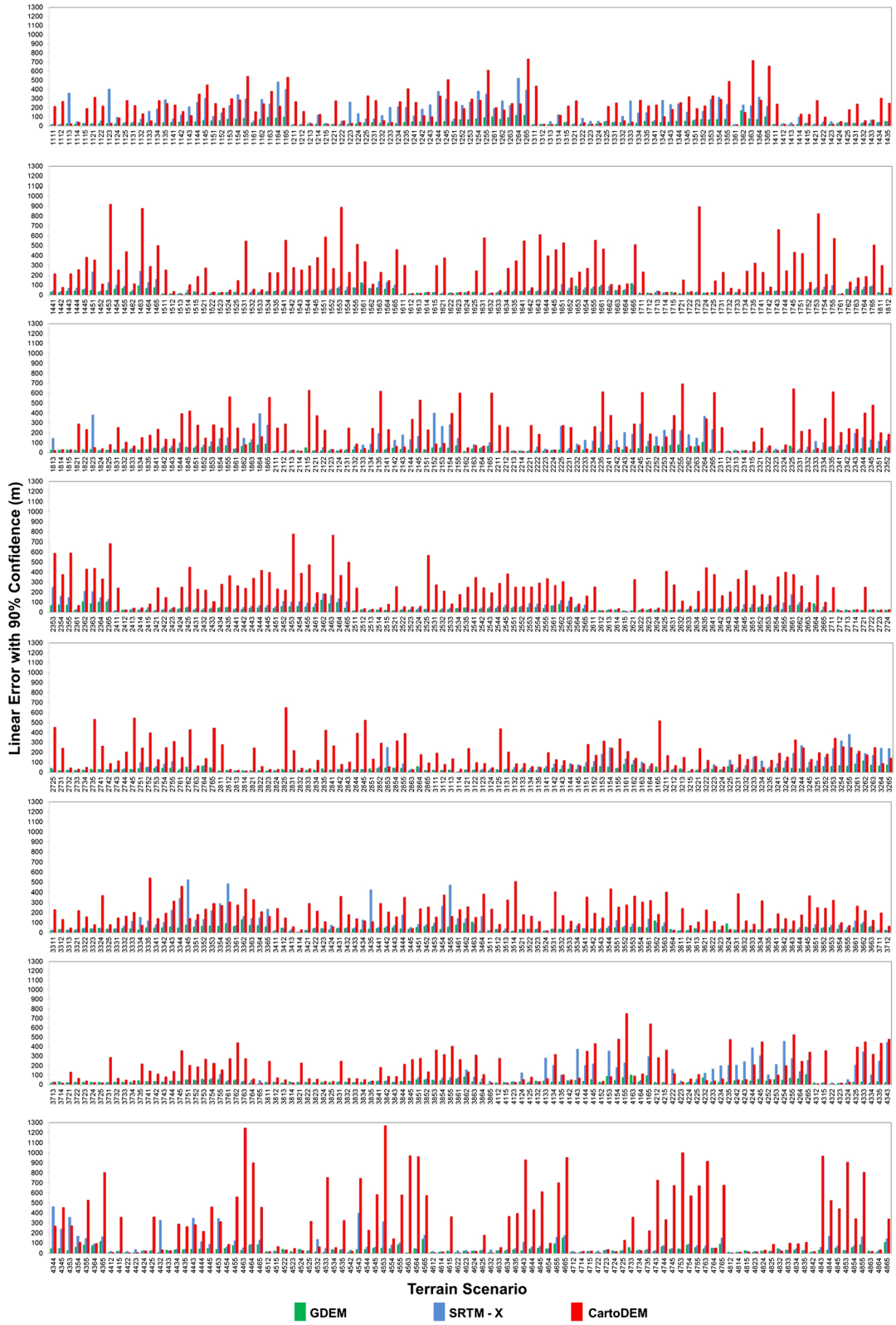
Linear Error with 90% Confidence (m)
Terrain Scenario
GDEM
SRTM - X
CartoDEM

◀ Figure 14
LE90 for various terrain scenarios. *Y* axis represents the linear error with 90 % confidence in meter. On *X* axis, the four numbers in each code represent class number for land cover, aspect, slope and elevation, respectively

the DEMs. Different combinations of these parameters give actual estimates of error. Usually the error in elevation increases with increasing altitude and slope. The vertical accuracies calculated for all three DEMs exceeded the mission specifications in high altitudes. ASTER GDEM V2 performed the best while CartoDEM gave poor vertical accuracies in the mountains. The main problems with SRTM X-band DEM were the voids or discontinuity in elevation due to layover and foreshortening effect on the microwave data.

Overall, ASTER GDEM V2 and CartoDEM showed underestimation of height while SRTM X-band DEM showed slight overestimation related to ADS80 DEM (Table 4). The positive and negative biases again vary with terrain scenarios. The findings of the study are important to understand the error associated with freely available DEMs with respect to a highly accurate ADS80 DEM. The study also depicts the terrain-based characteristics of the DEM error for various slopes, aspects, elevations and land cover. The study suggests that these freely available elevation models can be very useful for studying terrain parameters in high mountains, provided we are aware of the errors associated with them.

Based on accuracy achieved for different land cover classes (Table 8), we can say that source of error in the stereo photogrammetric-based DEMs (ASTER GDEM V2 and CartoDEM) was snow and ice and within the microwave-based SRTM X-band DEM was barren or exposed rocks followed by snow and ice. Interestingly, the presence of vegetation had less effect on accuracies of all these DEMs. Aerial survey in peak winter when most of the mountainous slopes are covered with snow should, therefore, be avoided to bypass such errors. But unlike land cover, the influence of the slope gradient on DEMs accuracy cannot be mitigated prior to sampling. When talking about over and underestimation of elevation, another interesting thing to note in Table 5 is that optical stereoscopic DEMs show overestimation in the lower slopes (up to 30°) and underestimation in higher slopes. On the contrary, the microwave-based SRTM X-band DEM shows underestimation till 30° and overestimation beyond that. CartoDEM still needs refinement on the part of producers for applications in the high mountains as the error exceeds the claimed one by a big margin.

References

Aguilar, F. J., Mills, J. P., Delgado, J., Aguilar, M. A., Negreiros, J., & Pérez, J. L. (2010a). *Modelling vertical error in LiDAR-derived digital elevation models*. ISPRS Journal of Photogrammetry & Remote Sensing, *65*, 103–110.

Aguilar, F. J., Fernández, I., Aguilar, M.A., Pérez, J. L., Delgado, J., & Negreiros, J.G. (2010b). *Shaded-reliefs matching as an efficient technique for 3d geo-referencing of historical Digital Elevation Models*. International Archives of the Photogrammetry, Remote Sensing and Spatial Information Science, Kyoto Japan, *38*(8), 1002–1007.

Arefi, H., & Reinartz, P. (2011). *Accuracy Enhancement of ASTER Global Digital Elevation Models Using ICESat Data*. Remote Sensing, *3*, 1323–1343.

Baghdadi, N., Lemarquand, N., Abdallah, H., & Bailly, J. S. (2011). *The Relevance of GLAS/ICESat Elevation Data for the Monitoring of River Networks*. Remote Sensing, *3*, 708–720.

Bhatt, S. & Ahmed, S.A. (2014). *Morphometric analysis to determine floods in the Upper Krishna basin using Cartosat DEM*. Geocarto International, *29*(8). DOI: 10.1080/10106049.2013.868042.

Chang, K.-t., & Tsai, B.-w. (1991). *The Effect of DEM Resolution on Slope and Aspect Mapping*. Cartography and Geographic Information Systems, *18*(1), 69–77.

Chen, Q. (2010). *Assessment of terrain elevation derived from satellite laser altimetry over mountainous forest areas using airborne LiDAR data*. ISPRS Journal of Photogrammetry & Remote Sensing, *65*, 111–122.

Czubski, K., Kozak, J., & Kolecka, N. (2013). Accuracy of SRTM-X and ASTER Elevation Data and its Influence on Topographical and Hydrological Modeling: Case Study of the pieniny Mts. in Poland. *International Journal of Geoinformatics*, *9*(2), 7–14.

Farr, T. G., Rosen, P. A., Caro, E., Crippen, R., Duren, R., Hensley, S., Kobrick, M., Paller, M., Rodriguez, E., Roth, L., Seal, D., Shaffer, S., Shimada, J., Umland, J., Werner, M., Oskin, M., Burbank, D., & Alsdorf, D. (2007). *The shuttle radar topography mission*. Reviews of Geophysics, *45*, 1–33.

Gianinetto, M. (2009). *Evaluation of Cartosat-1: Multi-Scale Digital Surface Modelling Over France*. Sensors, *9*, 3269–3288.

Gong, J., Li, Z., Zhu, Q., Sui, H., & Zhou, Y. (2000). *Effects of Various Factors on the Accuracy of DEMs: An Intensive Experimental Investigation*. Photogrammetric Engineering & Remote Sensing. *66*(9), 1113–1117.

Gorokhovich, Y., & Voustianiouk, A. (2006). *Accuracy assessment of the processed SRTM-based elevation data by CGIAR using field data from USA and Thailand and its relation to the*

terrain characteristics. Remote Sensing of Environment, *104*, 409–415.

Greenwalt, C., & Shultz, M. (1968). *Principles of Error Theory and Cartographic Applications.* St. Louis, MO: Aeronautical Chart and Information Center.

Gupta, R.D., Singh, M. K., Snehmani, & Ganju, A. (2014). *Validation of SRTM X band DEM over Himalayan Mountain*. The International Archives of the Photogrammetry, Remote Sensing and Spatial Information Sciences, *XL*-4. DOI: 10.5194/isprsarchives-XL-4-71-2014.

Hirano, A., Welch, R., & Lang, H. (2003). *Mapping from ASTER stereo image data: DEM validation and accuracy assessment*. ISPRS Journal of Photogrammetry & Remote Sensing, *57*, 356–370.

Hoffmann, J., & Walter, D. (2006). *How complementary are SRTM-X and -C Band Digital Elevation Models*? Photogrammetric Engineering & Remote Sensing, *72*(3), 261–268.

Höhle, J., & Höhle, M. (2009). *Accuracy assessment of digital elevation models by means of robust statistical methods*. ISPRS Journal of Photogrammetry & Remote Sensing, *64*, 398–406.

Holmes, K., Chadwick, O., & Kyriakidis, P. (2000). *Error in a USGS 30-meter digital elevation model and its impact on terrain modeling*. Journal of Hydrology, *233*, 154-173.

Huss, M., Farinotti, D., Bauder, A., & Funk, M. (2008). *Modelling runoff from highly glacierized alpine drainage basins in a changing climate*. Hydrological Processes, *22*, 3888–3902.

Jones, K. H. (1998). *A comparison of algorithms used to compute hill slope as a property of the DEM*. Computers & Geosciences, *24*(4), 315–323.

Kaab, A. (2005). *Combination of SRTM3 and repeat ASTER data for deriving alpine glacier flow velocities in the Bhutan Himalaya*. Remote Sensing of Environment, *94*, 463–474.

Kiel, B., Alsdorf, D., & LeFavour, G. (2006). *Capability of SRTM C- and X-band DEM Data to Measure Water Elevations in Ohio and the Amazon*. Photogrammetric Engineering & Remote Sensing, *72*(3), 1–8.

Koch, A., Heipke, C., & Lohmann, P. (2002). *Analysis of SRTM DTM methodology and practical results*. Symposium on Geospatial Theory, Processing and Applications.Commission IV, WG IV/6, pp. 1–6. Ottawa: ISPRS.

Kolecka, N., & Kozak, J. (2013). *Assessment of the Accuracy of SRTM C- and X-Band High Mountain Elevation Data: a Case Study of the Polish Tatra Mountains.* Pure and Applied Geophysics, DOI 10.1007/s00024-013-0695-5.

Krupnlk, A. (2000). *Accuracy Assessment of Automatically Derived Digital Elevation Models from SPOT Images.* Photogrammetric Engineering & Remote Sensing, *66*(8), 1017–1023.

Li, P., Shi, C., Li, Z., Muller, J.-P., Drummond, J., Li, X., Li, T., Li, Y., & Liu, J. (2013). *Evaluation of ASTER GDEM using GPS benchmarks and SRTM in China*. International Journal of Remote Sensing, *34*(5), 1744–1771.

Maathuis, B. H. P., & Wang, L. (2006). *Digital Elevation Model Based Hydro-processing*. Geocarto International, *21*(1), 21–26.

Martha, T. R., Kerle, N., Jetten, V., Westen, C. J., & Kumar, K. V. (2010). *Landslide Volumetric Analysis Using Cartosat-1-Derived DEMs*. IEEE Geoscience and Remote Sensing Letters, *7*(3), 582–586.

Maune, D. F., Kopp, S. M., Crawford, C. A., & Zervas, C. E. (2001). Introduction. In D. F. Maune (Ed.), *Digital Elevation Model Technologies and Applications: The DEM Users Manual.* Bethesda, Maryland: American Society for Photogrammetry and Remote Sensing, 537 pp.

Miliaresis, G. C., & Paraschou, C. V. (2005). *Vertical accuracy of the SRTM DTED level 1 of Crete*. International Journal of Applied Earth Observation & Geoinformation, *7*, 49–59.

Mukherjee, S., Joshi, P., Mukherjee, S., Ghosh, A., Garg, R., & Mukhopadhyay, A. (2013). *Evaluation of vertical accuracy of open source Digital Elevation Model (DEM)*. International Journal of Applied Earth Observation and Geoinformation, *21*, 205–217.

Muralikrishnan, S., B. Narender, Reddy, S., & Pillai, A. (2011). *Evaluation of Indian National DEM from Cartosat-1 Data.* Indian Space Research Organisation, National Remote Sensing Center, Hyderabad-625.

Muralikrishnan, S., Pillai, A., Narender, B., Reddy, S., Venkataraman, V. R., & Dadhwal, V. K. (2013). *Validation of Indian National DEM from Cartosat-1 Data*. Journal of Indian Society of Remote Sensing, *41*(1), 1–13.

Ni, W., Sun, G., Zhang, Z., Guo, Z., & He, Y. (2014). *Co-Registration of Two DEMs: Impacts on Forest Height Estimation from SRTM and NED at Mountainous Areas.* IEEE Geoscience and Remote Sensing Letters. *11*(1), 273–277.

Niel, T. G., McVicar, T. R., Li, L., Gallant, J. C., & Yang, Q. (2008). *The impact of misregistration on SRTM and DEM image differences*. Remote Sensing of Environment, *112*, 2430–2442.

Pandit, A., Ramsankaran, R., & Rao, Y.S. (2014). *Generation and Validation of the Interferometric SAR DEMsfrom TanDEM-X data for Gangotri and Hamtah Glaciers of Indian Himalayas*. Procedia Technology, *16*, 793–805.

Pradhan, B., & Youssef, A. M. (2010). *Manifestation of remote sensing data and GIS on landslide hazard analysis using spatial-based statistical models.* Arabian Journal of Geosciences, *3*, 319–326.

Rabus, B., Eineder, M., Roth, A., & Bamler, R. (2003). *The shuttle radar topography mission-a new class of digital elevation models acquired by spaceborne radar*. ISPRS Journal of Photogrammetry & Remote Sensing, *57*, 241–262.

Robinson, N., Regetz, J., & Guralnick, R. P. (2014). EarthEnvDEM90: *A nearly-global, void-free, multi-scale smoothed, 90 m digital elevation model from fused ASTER and SRTM data.* ISPRS Journal of Photogrammetry & Remote Sensing, *87*, 57–67.

Saxena, S., & Singh, H. P. (2005*). Some Estimators of the Dispersion Parameter of a Chi-distributed Radial Error with Applications to Target Analysis*. Austrian Journal of Statistics, *34*(1), 51–63.

Schneevoigt, N. J., Linden, S. v., Thamm, H.-P., & Schrott, L. (2008). *Detecting Alpine landforms from remotely sensed imagery. A pilot study in the Bavarian Alps*. Geomorphology, *93*, 104–119.

Singh, M. K., Snehmani, Gupta, R., Bhardwaj, A., Joshi, P. K., & Ganju, A. (2014). *High Resolution DEM Generation for Complex Snow Covered Indian Himalayan Region Using ADS80 Aerial Push-broom Camera: A First Time Attempt*. Arabian Journal of Geosciences. DOI: 10.1007/s12517-014-1299-9.

Snehmani, Bhardwaj, A., Singh, M. K., Gupta, R. D., Joshi, P. K., & Ganju, A. (2014). *Modeling hypsometric seasonal snow cover from observed meteorological parameters*. Journal of Spatial Science. DOI: 10.1080/14498596.2014.943310.

Snehmani, Singh, M. K., Gupta, R., & Ganju, A. (2013). *DTM Generation and Avalanche Hazard Mapping using Large Format*

Digital Photogrammetric Data and Geomatics Technique. Journal of Remote Sensing & GIS, *4*(2), 4–13.

Su, J., & Bork, E. (2006). *Influence of Vegetation, Slope, and Lidar Sampling Angle on DEM Accuracy.* Photogrammetric Engineering & Remote Sensing, *72*(11), 1265–1274.

Sun, G., Ranson, K., Kharuk, V., & Kovacs, K. (2003). *Validation of surface height from shuttle radar topography mission using shuttle laser altimeter*. Remote Sensing of Environment, *88*, 401–411.

Tachikawa, T., Kaku, M., Iwasaki, A., Gesch, D., Oimoen, M., Zhang, Z., Danielson, J., Krieger, T., Curtis, B., Haase, J., Abrams, M., Crippen, R., & Carabajal, C. (2011). *ASTER Global Digital Elevation Model Version 2 –Summary of Validation Results.* Summary of Validation Results, NASA Land Processes Distributed Active Archive Center and the Joint Japan-US ASTER Science Team.

Thornton, P. E., Running, S. W., & White, M. A. (1997). *Generating surfaces of daily meteorological variables over large regions of complex terrain.* Journal of Hydrology, *190*, 214–251.

Toschi, I., Rodríguez-González, P., Remondino, F., Minto, S., Orlandini, S., & Fuller, A. (2015). *Accuracy evaluation of a mobile mapping system with advanced statistical methods*. The International Archives of the photogrammetry, Remote Sensing and Spatial Information Sciences, XL-5/W4. DOI: 10.5194/isprsarchives-XL-5-W4-245-2015.

Yadav, S.K., Singh, S. K., Gupta, M., & Srivastava, P.K. (2014). Morphometric analysis of Upper Tons basin from Northern Foreland of Peninsular India using CARTOSAT satellite and GIS. *Geocarto International*, *29*(8), 895–914. DOI: 10.1080/10106049.2013.868043.

Zhang, S., Peterson, J., & Shan, J. (2004). *High quality 3D visualization for glacial cirque terrain*. Journal of Spatial Science, *49*(2), 75–86.

Zhang, W., & Montgomery, D. R. (1994). *Digital elevation model grid size, landscape representation, and hydrologic simulations.* Water Resources Research, *30*(4), 1019–1028.

(Received December 17, 2014, revised May 27, 2015, accepted June 2, 2015, Published online July 4, 2015)